An International Journal of Optimization and Control: Theories & Applications
ISSN: 2146-0957 eISSN: 2146-5703
Vol.x, No.x, pp.xx-xx (2026)
https://doi.org/10.36922/IJOCTA026310189

RESEARCH ARTICLE

Dynamics of tuberculosis via NSFD scheme with nonlinear incidence, relapse, reinfection, and saturated treatment

Moch. Fandi Ansori*

Department of Mathematics, Faculty of Science and Mathematics, Universitas Diponegoro, Semarang, Indonesia
mochfandiansori@lecturer.undip.ac.id

ARTICLE INFO

Article history:
Received: July 27, 2026
Revised: October 22, 2026
Accepted: October 23, 2026
Published Online: November 6, 2026

Keywords:
Tuberculosis
Nonstandard finite difference scheme
Saturated treatment
Backward bifurcation
Real data
Parameter estimation

AMS Classification 2010:
39A28; 92D30; 37N25

ABSTRACT

Tuberculosis (TB) remains one of the most prevalent infectious diseases worldwide and continues to pose a major public health challenge. This study presents a TB model using a nonstandard finite difference (NSFD) scheme that incorporates nonlinear incidence, relapse, reinfection, and saturated treatment effects. The discrete model is designed to preserve the key qualitative properties of the continuous system, including positivity, boundedness, and invariance of the feasible region. The disease-free and endemic equilibria are analyzed, and their local stability conditions are established using the Jury criterion. The basic reproduction number is derived and is consistent with that of the corresponding continuous model. Furthermore, the bifurcation analysis reveals that the model can exhibit either forward or backward bifurcation, indicating the possibility of bistability and disease persistence even when the basic reproduction number is less than one. To better reflect real-world dynamics, the model parameters are estimated using TB incidence data from Indonesia for the period 2000–2024. Numerical simulations, including the dynamical behavior around equilibria, global sensitivity analysis, epidemiological outcome sensitivity, and bifurcation diagrams, further support the analytical results. The robustness of the proposed NSFD scheme and its performance relative to classical numerical methods are also examined. The results highlight the importance of incorporating treatment saturation and nonlinear transmission in understanding TB dynamics while providing a reliable discrete-time modeling framework.

CC BY

1. Introduction

Tuberculosis (TB) remains one of the most significant infectious diseases worldwide and continues to pose a major public health challenge, particularly in middle- and low-income countries. Caused by *Mycobacterium tuberculosis*, the disease primarily affects the lungs but can also involve other organs, resulting in extrapulmonary TB.[1–3] Transmission occurs through airborne droplets generated by coughing, sneezing, or speaking, with the risk being higher in crowded and poorly ventilated environments.[1,3] TB imposes a substantial global burden of morbidity and mortality each year. The burden falls disproportionately on middle- and low-income countries, where malnutrition, poverty, and limited access to healthcare are widespread.[4–6] Global control efforts are being implemented through the Directly Observed Treatment, Short-course (DOTS) strategy and the End TB Strategy of the World Health Organization (WHO). Nevertheless, the disease burden remains high because of various epidemiological and socioeconomic challenges.[7,8]

The persistence of TB is driven by multiple factors, including relapse, reinfection, drug resistance, and limited healthcare capacity. These

*Corresponding Author

factors give rise to highly nonlinear transmission dynamics that are difficult to investigate using purely empirical approaches. Moreover, the emergence of multidrug-resistant strains,[9–11] TB/HIV co-infection,[12–14] and limitations in healthcare systems, such as inadequate diagnostic capacity and treatment follow-up, further complicate disease control.[15] These challenges highlight the need for mathematical models that can capture the key mechanisms governing TB dynamics and provide insights into effective intervention strategies.

Mathematical modeling has become an indispensable tool for studying TB transmission and control. Various modeling approaches, including ordinary differential equation models and fractional-order models, have been developed to represent key biological and epidemiological processes.[16–18] Other models have demonstrated that mechanisms such as relapse and reinfection play an important role in sustaining disease transmission, while social and environmental factors significantly influence its spread.[19–21] Furthermore, several modeling studies have suggested that interventions such as vaccination, early diagnosis, and improved treatment adherence can substantially reduce TB incidence, although their effectiveness depends strongly on the underlying system dynamics and parameter interactions.[18,22–27]

Most classical TB models rely on simplifying assumptions, such as linear incidence and unlimited treatment capacity, which may not adequately represent real-world conditions. In practice, healthcare systems are resource-constrained and often have limited treatment capacity, which can substantially alter disease dynamics. Models incorporating saturated treatment have shown that such limitations can lead to complex dynamical behaviors, including backward bifurcation and bistability, where the disease persists despite the basic reproduction number remaining below unity.[28–30] Moreover, insufficient healthcare resources may promote the emergence of drug-resistant strains and reduce the effectiveness of intervention strategies, highlighting the importance of incorporating nonlinear incidence and treatment capacity constraints into TB models.[31–33]

In addition to model formulation, the choice of numerical discretization plays a crucial role in the accurate simulation of epidemiological systems. Standard finite difference methods often fail to preserve critical qualitative properties of the continuous model, such as boundedness, stability, and positivity, which may lead to unrealistic numerical solutions.[34,35] These limitations have motivated the use of the nonstandard finite difference (NSFD) scheme, which is designed to preserve the dynamical consistency of the original system.[36–39] NSFD schemes preserve key qualitative features, such as the stability of equilibria and the positivity of solutions, while allowing relatively large time steps without compromising numerical stability.[40–43] These properties make NSFD schemes particularly suitable for epidemiological models, where preserving biological feasibility and numerical stability is essential.[44,45] Reliable finite difference schemes are therefore essential for such simulations.[46,47]

Motivated by these considerations, this study introduces an NSFD scheme for a TB model that incorporates relapse, reinfection, nonlinear incidence, and saturated treatment. Our model is based on the study by Aldila,[20] which considered a susceptible–infected–recovered TB model with relapse, reinfection, and nonlinear incidence. The model is given in (1), and its formulation and derivation are presented in the next section. In this paper, we extend the TB model of[20] by incorporating saturated treatment and developing an NSFD scheme. This constitutes the first novelty of our work. The discrete model is constructed to preserve the key qualitative properties of the continuous system. Second, we establish the positivity and invariance of the feasible region of the NSFD TB model, analyze the local stability of the equilibria, and investigate bifurcation phenomena. In particular, we demonstrate that the model is capable of exhibiting backward bifurcation. Third, we estimate the model parameters using real-world data and provide several numerical simulations to validate the theoretical results and to examine the robustness of the proposed NSFD scheme. From a practical perspective, the proposed NSFD scheme can support computational studies of TB models, enabling more reliable evaluation of public health intervention strategies.

Fractional-order models have recently attracted considerable attention in TB modeling because they can incorporate memory and hereditary effects associated with disease progression and treatment history.[48–52] Such models are particularly useful when past states substantially influence the current dynamics. Nevertheless, the

objective of the present study is not to investigate memory effects but to develop and analyze an NSFD scheme that preserves the essential qualitative properties of the underlying epidemic model. A classical integer-order formulation provides a well-established framework for these theoretical analyses and enables direct comparison with the continuous model of Aldila,[20] which serves as the basis of the present work. Although fractional-order models may offer a richer description of certain epidemiological processes, they generally introduce additional mathematical complexity. Therefore, the classical-order formulation adopted in this study is appropriate for achieving the objectives of developing a dynamically consistent NSFD scheme and investigating its qualitative dynamics.

The structure of the paper is as follows. Section 2 outlines the governing equations of the model by first introducing the previous model with relapse, reinfection, and nonlinear incidence, followed by its extension incorporating saturated treatment and its dimensionless formulation. Section 3 presents the NSFD scheme for the proposed model. Section 4 analyzes the NSFD model, including the basic properties, the disease-free equilibrium and its local stability in relation to the basic reproduction number, the endemic equilibrium, and the potential for both forward and backward bifurcations. To confirm the analytical results, Section 5 presents the model parameter estimation together with several numerical simulations, including the dynamics around the equilibria, sensitivity analysis of the basic reproduction number, epidemiological outcomes, bifurcation diagrams, and the robustness of the NSFD scheme in comparison with classical numerical methods. Finally, Section 6 presents the conclusions.

2. Mathematical model

This section begins by recalling the time-continuous TB model from our previous study, which is formulated as a susceptible–infected–recovered (SIR) system with nonlinear incidence, relapse, and reinfection. We then extend this framework by incorporating a saturated treatment effect to represent the limited capacity of healthcare systems as the number of infected individuals increases. Finally, we derive the corresponding dimensionless form of the model.

2.1. The previous SIR tuberculosis model

For every time t, let $S(t)$ denote the number of susceptible individuals, $I(t)$ the number of infected individuals, and $R(t)$ the number of treated/recovered individuals who have left the active infectious state. The total population is

$$N(t) = S(t) + I(t) + R(t).$$

Following the study of Aldila,[20] the population is divided into these three compartments, and the disease transmission process incorporates nonlinear incidence, relapse of recovered individuals, and reinfection of r ecovered individuals.

Individuals enter the susceptible class through recruitment at a constant rate Λ, while all individuals experience natural death at rate μ. New infections arise through effective contact between susceptible and infected individuals. To capture the increased risk of transmission as the number of infective individuals grows, the incidence is assumed to be

$$\beta_1(1+\nu I)I,$$

where β_1 is the baseline transmission coefficient and ν is a correction parameter. The nonlinear factor $1+\nu I$ is introduced to represent population-level amplification of effective exposure that may arise from clustering of infectious individuals, repeated exposure in high-transmission settings, or other unobserved heterogeneities in contact intensity.

Infectious individuals leave the active infectious class following successful treatment at rate γ. Recovered individuals may lose immunity and relapse to the infected class. If α denotes the relapse rate and $p \in (0,1)$ is the proportion of recovered individuals who relapse, then $p\alpha R$ represents the flow from R back to I, while $(1-p)\alpha R$ represents those who leave the relapse process without returning to the infected class. In addition, recovered individuals may become reinfected through contact with infective individuals, with reinfection rate

$$\beta_2(1+\nu I)IR,$$

where β_2 is the reinfection coefficient.

Thus, the TB model is given by[20]

$$\begin{aligned}
\frac{dS}{dt} &= \Lambda - \beta_1(1+\nu I)IS + (1-p)\alpha R - \mu S,\\
\frac{dI}{dt} &= \beta_1(1+\nu I)IS - \gamma I + p\alpha R\\
&\quad + \beta_2(1+\nu I)IR - \mu I,\\
\frac{dR}{dt} &= \gamma I - \alpha R - \beta_2(1+\nu I)IR - \mu R.
\end{aligned} \tag{1}$$

Since

$$\frac{dN}{dt} = \Lambda - \mu N,$$

the total population converges to the constant level

$$N = \frac{\Lambda}{\mu}.$$

Under this assumption, the model can be nondimensionalized and reduced to a lower-dimensional system.

2.2. The proposed model with saturated treatment

Although the recovery term γI in system (1) is mathematically convenient, it assumes that the treatment capacity increases proportionally with the number of infective individuals. In practice, however, treatment resources, such as medical staff, diagnostic facilities, drug availability, and patient monitoring systems, are limited. Consequently, the healthcare system may become overburdened when the number of infected individuals increases substantially, causing the effective treatment rate to no longer increase linearly with I.

To account for this effect, we replace the linear recovery term γI with the saturated treatment function

$$\frac{\gamma I}{1+aI},$$

where $a > 0$ measures the level of treatment saturation. The saturated treatment represents the rate at which actively infectious individuals successfully complete or respond to treatment and move to the post-treatment class. Treatment saturation reflects limitations in diagnostic, treatment, and follow-up capacity. When I is small, the term behaves approximately as γI, whereas for large I, the treatment effect increases more slowly because of limited healthcare capacity. See, for example,[28,53–58] for studies highlighting the role of saturated treatment in tuberculosis modeling.

Accordingly, the modified TB model is formulated as

$$\begin{aligned}
\frac{dS}{dt} &= \Lambda - \beta_1(1+\nu I)IS + (1-p)\alpha R - \mu S,\\
\frac{dI}{dt} &= \beta_1(1+\nu I)IS - \frac{\gamma I}{1+aI} + p\alpha R\\
&\quad + \beta_2(1+\nu I)IR - \mu I,\\
\frac{dR}{dt} &= \frac{\gamma I}{1+aI} - \alpha R - \beta_2(1+\nu I)IR - \mu R.
\end{aligned} \tag{2}$$

The initial conditions are assumed to be

$$S(0) \geq 0, \qquad I(0) > 0, \qquad R(0) \geq 0.$$

Summing the equations in (2) yields

$$\frac{dN}{dt} = \Lambda - \mu N.$$

Hence, as in the previous model, if the total population remains constant, then

$$N = \frac{\Lambda}{\mu}.$$

2.3. Dimensionless form of the model

To obtain a dimensionless system, we introduce the normalized variables

$$x_1 = \frac{S}{N}, \qquad x_2 = \frac{I}{N}, \qquad x_3 = \frac{R}{N},$$

so that

$$x_1 + x_2 + x_3 = 1.$$

We further define the dimensionless parameters

$$b_1 = \beta_1 N, \quad b_2 = \beta_2 N, \quad v = \nu N, \quad \tilde{a} = aN.$$

Since $I = Nx_2$, the saturated treatment term becomes

$$\frac{\gamma I}{1+aI} = \frac{\gamma N x_2}{1+aNx_2} = \frac{\gamma N x_2}{1+\tilde{a}x_2}.$$

Dividing system (2) by N and using $\Lambda = \mu N$, we obtain

$$\begin{aligned}
\frac{dx_1}{dt} &= \mu - b_1(1+vx_2)x_1x_2 + (1-p)\alpha x_3 - \mu x_1,\\
\frac{dx_2}{dt} &= b_1(1+vx_2)x_1x_2 - \frac{\gamma x_2}{1+\tilde{a}x_2}\\
&\quad + p\alpha x_3 + b_2(1+vx_2)x_2x_3 - \mu x_2,\\
\frac{dx_3}{dt} &= \frac{\gamma x_2}{1+\tilde{a}x_2} - \alpha x_3 - b_2(1+vx_2)x_2x_3 - \mu x_3.
\end{aligned} \tag{3}$$

Using the relation

$$x_1 = 1 - x_2 - x_3,$$

the three-dimensional system (3) can be reduced to the following two-dimensional system:

$$\begin{aligned}
\frac{dx_2}{dt} &= b_1(1-x_2-x_3)(1+vx_2)x_2 - \frac{\gamma x_2}{1+\tilde{a}x_2}\\
&\quad + p\alpha x_3 + b_2(1+vx_2)x_2x_3 - \mu x_2,\\
\frac{dx_3}{dt} &= \frac{\gamma x_2}{1+\tilde{a}x_2} - \alpha x_3 - b_2(1+vx_2)x_2x_3 - \mu x_3.
\end{aligned} \tag{4}$$

The dimensionless system (4) serves as the basis for constructing the discrete-time model in the following section using the nonstandard finite difference scheme.

3. Nonstandard finite difference scheme

This section develops a discrete-time version of system (4) using the nonstandard finite difference (NSFD) method proposed by Mickens.[36–39] The scheme is designed to preserve the key qualitative properties of the continuous model, including the invariance of the feasible region and the positivity of solutions.

Let $h > 0$ denote the time step, and let $t_n = nh$, $n = 0, 1, 2, \ldots$. Define

$$x_{2,n} \approx x_2(t_n), \qquad x_{3,n} \approx x_3(t_n).$$

Following Mickens' approach, the time derivative is approximated by

$$\frac{dx}{dt} \approx \frac{x_{n+1} - x_n}{\phi(h)},$$

where the denominator function is chosen as

$$\phi(h) = 1 - e^{-h},$$

which is a standard nonlocal denominator satisfying

$$\phi(h) = h + \mathcal{O}(h^2) \quad \text{and} \quad 0 < \phi(h) < 1.$$

This choice preserves the consistency of the finite difference approximation while allowing relatively large time steps and maintaining important qualitative properties of the continuous system, such as positivity and boundedness of the solutions.

To ensure dynamical consistency, we separate each equation into gain and loss terms. For system (4), define

$$\begin{aligned} F_n &= b_1(1 - x_2 - x_3)(1 + vx_2)x_2 + p\alpha x_3 \\ &\quad + b_2(1 + vx_2)x_2x_3, \\ H_n &= \frac{\gamma x_{2,n}}{1 + \tilde{a}x_{2,n}}, \\ G_n &= \mu + \frac{\gamma}{1 + \tilde{a}x_{2,n}}, \\ K_n &= \alpha + \mu + b_2(1 + vx_{2,n})x_{2,n}. \end{aligned} \tag{5}$$

Here, F_n and H_n represent the nonnegative gain terms, whereas G_n and K_n represent the corresponding loss rates.

The NSFD scheme is then constructed as

$$\begin{aligned} x_{2,n+1} &= \frac{x_{2,n} + \phi(h)\, F_n}{1 + \phi(h)\, G_n}, \\ x_{3,n+1} &= \frac{x_{3,n} + \phi(h)\, H_n}{1 + \phi(h)\, K_n}. \end{aligned} \tag{6}$$

System (6) defines a nonlinear discrete dynamical system, which will be analyzed in the subsequent sections.

4. Model analysis

This section investigates the equilibrium points of the discrete system (6), analyzes their local stability using the Jury criterion, examines the occurrence and direction of bifurcations, and discusses the global stability of the equilibria.

4.1. Positivity and invariant region

This subsection demonstrates that the NSFD scheme preserves the essential qualitative properties of the continuous model, namely the positivity of the state variables and the invariance of the biologically feasible region.

Theorem 1. *Let*

$$\begin{aligned} \Omega_r = \big\{ &(x_2, x_3) \in \mathbb{R}^2_+ : 0 \le x_2 \le 1, \\ &0 \le x_3 \le r(1 - x_2) \big\}, \end{aligned}$$

where $0 < r < 1$ and define $d_r = (1 - r)b_1 + rb_2$. Suppose that $b_2 \ge b_1$ and

$$rp\alpha + (1 + v)d_r \le 1, \tag{7}$$

$$r \min\{\mu, \psi_0, \psi_1\} \ge \frac{(1 - r)\gamma}{\widetilde{a}}, \tag{8}$$

where

$$\begin{aligned} \psi_0 &= (\alpha + \mu)(1 - rp\alpha) - rp\alpha, \\ \psi_1 &= (\alpha + \mu + b_2)\left[1 - rp\alpha - (1 + v)d_r\right] \\ &\quad - \left[rp\alpha + (1 + v)d_r\right]. \end{aligned}$$

If $(x_{2,0}, x_{3,0}) \in \Omega_r$, then $(x_{2,n}, x_{3,n}) \in \Omega_r$ for all $n \ge 0$ and $h > 0$. Consequently, Ω_r is positively invariant under the NSFD scheme (6).

Proof. Assume that $(x_{2,n}, x_{3,n}) \in \Omega_r$. Since $0 \le x_{3,n} \le r(1 - x_{2,n}) \le 1 - x_{2,n}$, we have $F_n \ge 0$, $H_n \ge 0$, $G_n > 0$, $K_n > 0$. Hence, from system (6),

$$x_{2,n+1} \ge 0, \qquad x_{3,n+1} \ge 0.$$

It remains to prove $x_{3,n+1} \le r(1 - x_{2,n+1})$. For fixed $x_{2,n}$, we have

$$\frac{\partial F_n}{\partial x_{3,n}} = p\alpha + (b_2 - b_1)(1 + vx_{2,n})x_{2,n}.$$

If $b_2 \ge b_1$, then $\frac{\partial F_n}{\partial x_{3,n}} \ge 0$, and consequently

$$\frac{\partial x_{2,n+1}}{\partial x_{3,n}} = \frac{\phi(h)}{1 + \phi(h)G_n} \frac{\partial F_n}{\partial x_{3,n}} \ge 0.$$

Also, we have

$$\frac{\partial x_{3,n+1}}{\partial x_{3,n}} = \frac{1}{1 + \phi(h)K_n} > 0.$$

Thus, for fixed $x_{2,n}$, both $x_{2,n+1}$ and $x_{3,n+1}$ are nondecreasing functions of $x_{3,n}$. Therefore, $r(1 - x_{2,n+1}) - x_{3,n+1}$ is nonincreasing with respect to $x_{3,n}$. Its minimum over $0 \le x_{3,n} \le r(1 - x_{2,n})$ is consequently attained at $x_{3,n} = r(1 - x_{2,n})$. Hence, it is sufficient to verify the invariance condition on this boundary.

Let $x = x_{2,n}$. On the boundary $x_{3,n} = r(1 - x_{2,n})$, we have $F_n = (1 - x)\left[d_r(1 + vx)x + rp\alpha\right]$. After substituting into system (6), the inequality

$$x_{3,n+1} \le r(1 - x_{2,n+1})$$

is equivalent to

$$A(x) + \phi(h)B(x) \ge 0,$$

where

$$\begin{aligned} A(x) &= r\left[(1 - x)K_n + xG_n - F_n\right] - H_n, \\ B(x) &= rK_n(G_n - F_n) - H_nG_n. \end{aligned}$$

Using the expressions for F_n, G_n, H_n, and K_n, we obtain

$$\begin{aligned} A(x) &= r\mu + r\alpha(1 - rp)(1 - x) \\ &\quad + r(1 - r)(b_2 - b_1)(1 + vx)x(1 - x) \\ &\quad - \frac{(1 - r)\gamma x}{1 + \widetilde{a}x}. \end{aligned}$$

Hence, by assumption (8), we have

$$A(x) \geq r\mu - \frac{(1-r)\gamma}{\widetilde{a}} \geq 0.$$

Furthermore,

$$A(x) + B(x) \geq r(1-x)E(x) + r\mu x - \frac{(1-r)\gamma}{\widetilde{a}},$$

where

$$E(x) = (\alpha + \mu + b_2 x)\left[1 - rp\alpha - (1+v)d_r x\right] - \left[rp\alpha + (1+v)d_r x\right].$$

Using assumption (7), $E(x)$ is concave on $[0,1]$ and

$$E(x) \geq \min\{\psi_0, \psi_1\}.$$

Therefore,

$$A(x) + B(x) \geq r\min\{\mu, \psi_0, \psi_1\} - \frac{(1-r)\gamma}{\widetilde{a}} \geq 0.$$

Since $0 < \phi(h) < 1$, the inequalities $A(x) \geq 0$ and $A(x) + B(x) \geq 0$ imply

$$A(x) + \phi(h)B(x) \geq 0.$$

Thus,

$$x_{3,n+1} \leq r(1 - x_{2,n+1}),$$

and hence $(x_{2,n+1}, x_{3,n+1}) \in \Omega_r$. The conclusion follows by induction. □

4.2. Local stability of the disease-free equilibrium

An equilibrium $E^* = (x_2^*, x_3^*)$ of system (6) satisfies

$$x_{2,n+1} = x_{2,n} = x_2^*, \qquad x_{3,n+1} = x_{3,n} = x_3^*.$$

Substituting into (6), we obtain

$$x_2^* = \frac{x_2^* + \phi(h)\,F(x_2^*, x_3^*)}{1 + \phi(h)\,G(x_2^*)},$$
$$x_3^* = \frac{x_3^* + \phi(h)\,H(x_2^*)}{1 + \phi(h)\,K(x_2^*)},$$

which simplifies to

$$\begin{aligned} 0 &= F(x_2^*, x_3^*) - G(x_2^*)\,x_2^*, \\ 0 &= H(x_2^*) - K(x_2^*)\,x_3^*. \end{aligned} \tag{9}$$

The discrete model and the corresponding continuous system share the same equilibrium points. The disease-free equilibrium (DFE) is given by

$$E_0 = (0,0).$$

We now examine the local stability of the DFE $E_0 = (0,0)$ for the discrete system (6). For simplicity, let

$$\phi = \phi(h) = 1 - e^{-h}.$$

Differentiating the right-hand sides of system (6) and evaluating them at the DFE $E_0 = (0,0)$, we obtain the Jacobian matrix. Hence, after straightforward differentiation and simplification, the Jacobian matrix at E_0 is

$$J(E_0) = \begin{pmatrix} \dfrac{1+\phi b_1}{1+\phi(\mu+\gamma)} & \dfrac{\phi p\alpha}{1+\phi(\mu+\gamma)} \\ \dfrac{\phi\gamma}{1+\phi(\alpha+\mu)} & \dfrac{1}{1+\phi(\alpha+\mu)} \end{pmatrix}. \tag{10}$$

For simplicity, define

$$a = \frac{1+\phi b_1}{1+\phi(\mu+\gamma)}, \quad b = \frac{\phi p\alpha}{1+\phi(\mu+\gamma)},$$
$$c = \frac{\phi\gamma}{1+\phi(\alpha+\mu)}, \quad d = \frac{1}{1+\phi(\alpha+\mu)}.$$

The trace and determinant of $J(E_0)$ are

$$\operatorname{Tr} J(E_0) = a + d, \qquad \det J(E_0) = ad - bc.$$

The characteristic polynomial of $J(E_0)$ takes the form

$$\lambda^2 - (a+d)\lambda + (ad - bc) = 0.$$

Its discriminant is

$$\Delta = (a-d)^2 + 4bc > 0.$$

Hence, both eigenvalues are real.

According to the Jury stability criterion, E_0 is locally asymptotically stable if and only if the following conditions hold:

$$1-(a+d)+(ad-bc) > 0,\ 1+(a+d)+(ad-bc) > 0,$$
$$1 - (ad - bc) > 0.$$

The stability conditions are derived from the general Jury stability criterion.[59] For a second-order characteristic polynomial, these conditions reduce to the above inequalities.

Denote the common denominator of $\operatorname{Tr} J(E_0)$ and $\det J(E_0)$ by

$$D = \big(1 + \phi(\mu+\gamma)\big)\big(1 + \phi(\alpha+\mu)\big).$$

Clearly, $D > 0$.

Next,

$$\begin{aligned} &1 - (a+d) + (ad - bc) \\ &= \frac{1}{D}\Big(\phi^2[(\alpha+\mu)(\mu+\gamma-b_1) - p\alpha\gamma]\Big), \\ &1 + (a+d) + (ad - bc) \\ &= \frac{1}{D}\Big(4 + 2\phi(b_1 + \alpha + 2\mu + \gamma) \\ &\quad + \phi^2[(\alpha+\mu)(\mu+b_1) + \mu\gamma + (1-p)\alpha\gamma]\Big), \\ &1 - (ad - bc) \\ &= \frac{1}{D}\Big(\phi(\alpha + 2\mu + \gamma - b_1) \\ &\quad + \phi^2[(\mu+\gamma)(\alpha+\mu) + p\alpha\gamma]\Big). \end{aligned}$$

Condition $1 - (a+d) + (ad - bc) > 0$ can be written as

$$(\alpha+\mu)(\mu+\gamma-b_1) - p\alpha\gamma > 0. \tag{11}$$

Observe that the condition $1 + (a+d) + (ad - bc) > 0$ always holds. Meanwhile, the condition

$1-(ad-bc)>0$ is equivalent to

$$(\alpha+2\mu+\gamma-b_1)+\phi[(\mu+\gamma)(\alpha+\mu)+p\alpha\gamma]>0. \quad (12)$$

If (11) holds, then (12) also holds. Therefore, condition (11) is sufficient for all three Jury inequalities.

Define the threshold parameter

$$\mathcal{R}_0=\frac{b_1(\alpha+\mu)}{(\gamma+\mu)(\alpha+\mu)-p\alpha\gamma}. \quad (13)$$

Then the condition (11) is equivalent to

$$\mathcal{R}_0<1.$$

Therefore, the following result holds.

Theorem 2. *The DFE of system* (6) $E_0=(0,0)$ *is locally asymptotically stable if* $\mathcal{R}_0<1$.

Remark 1. *For the corresponding continuous dimensionless system* (3)*, the next-generation matrix method*[60,61] *is used to derive* $\mathcal{R}_0$*. Considering the infected subsystem* (x_2,x_3) *at the DFE, linearization and separation of the new infection and transition terms yield the matrices*

$$\mathbb{F}=\begin{pmatrix} b_1 & 0\\ 0 & 0\end{pmatrix},\qquad \mathbb{V}=\begin{pmatrix} \gamma+\mu & -p\alpha\\ -\gamma & \alpha+\mu\end{pmatrix}.$$

Hence, $\mathcal{R}_0$ *equals the spectral radius of* $\mathbb{F}\mathbb{V}^{-1}$*, namely*

$$\mathcal{R}_0=\frac{b_1(\alpha+\mu)}{(\gamma+\mu)(\alpha+\mu)-p\alpha\gamma}.$$

Notably, this expression coincides exactly with the threshold parameter obtained for the NSFD scheme. This agreement shows that the NSFD discretization maintains the epidemiological threshold dynamics of the continuous model, ensuring consistency between both formulations.

Loss of stability occurs when one of the Jury stability conditions becomes an equality.

(i) Crossing through $\lambda=1$.

The condition

$$1-(a+d)+(ad-bc)=0$$

yields

$$(\alpha+\mu)(\mu+\gamma-b_1)-p\alpha\gamma=0,$$

or equivalently

$$b_1^*=\mu+\gamma-\frac{p\alpha\gamma}{\alpha+\mu}. \quad (14)$$

Thus, one eigenvalue satisfies $\lambda=1$ when $b_1=b_1^*$, or equivalently when $\mathcal{R}_0=1$.

(ii) Crossing through $\lambda=-1$.

The condition

$$1+(a+d)+(ad-bc)=0$$

cannot be satisfied for positive parameters and $h>0$. Hence, a flip bifurcation does not occur at E_0.

(iii) Neimark–Sacker bifurcation.

Since both eigenvalues are always real ($\Delta>0$), a complex-conjugate pair cannot arise. Therefore, a Neimark–Sacker bifurcation cannot occur at E_0. The results are summarized in the following theorem.

Theorem 3. *At the DFE* $E_0=(0,0)$*:*

(1) Stability is lost when $\mathcal{R}_0=1$.
(2) A flip bifurcation cannot occur.
(3) A Neimark–Sacker bifurcation cannot occur.

4.3. Endemic equilibrium

We now derive a scalar equation for the endemic equilibrium (EE), which is subsequently used to determine the direction of the bifurcation at $\mathcal{R}_0=1$.

Let $E^*=(x_2^*,x_3^*)$ denote the EE of system (6), where

$$x_2^*>0,\qquad x_3^*>0.$$

From (9), the equilibrium coordinates satisfy

$$\begin{aligned}&\big(b_1(1-x_2^*-x_3^*)+b_2x_3^*\big)(1+vx_2^*)x_2^*+p\alpha x_3^*\\&=\left(\mu+\frac{\gamma}{1+\tilde{a}x_2^*}\right)x_2^*,\\&\frac{\gamma x_2^*}{1+\tilde{a}x_2^*}=(\alpha+\mu+b_2(1+vx_2^*)x_2^*)\,x_3^*.\end{aligned} \quad (15)$$

From the second equation of (15), we obtain

$$x_3^*=\frac{\gamma x_2^*}{(1+\tilde{a}x_2^*)\,(\alpha+\mu+b_2(1+vx_2^*)x_2^*)}. \quad (16)$$

Substituting (16) into the first equation of (15), and letting

$$x=x_2^*,$$

we obtain the scalar equation

$$\begin{aligned}\mathcal{F}(x):=&(1+vx)\,b_1(1-x)(1+\tilde{a}x)\\&\times\Big(\alpha+\mu+b_2(1+vx)x\Big)\\&+(1+vx)(b_2-b_1)\gamma x+p\alpha\gamma\\&-\big(\mu(1+\tilde{a}x)+\gamma\big)\\&\times\Big(\alpha+\mu+b_2(1+vx)x\Big)=0.\end{aligned} \quad (17)$$

Therefore, every positive root $x=x_2^*$ of (17) determines an EE through (16).

Evaluating $\mathcal{F}(x)$ at $x=0$, we obtain

$$\mathcal{F}(0)=(\alpha+\mu)b_1+p\alpha\gamma-(\mu+\gamma)(\alpha+\mu).$$

Hence,

$$\mathcal{F}(0)=0\quad\Longleftrightarrow\quad b_1=b_1^*,$$

where

$$b_1^* = \mu + \gamma - \frac{p\alpha\gamma}{\alpha+\mu}. \tag{18}$$

This threshold coincides with that obtained from the local stability analysis of the DFE.

4.4. Bifurcation analysis

To determine the bifurcation direction, we analyze the EE branch near the DFE using a local expansion approach (see, e.g.,[62,63]). By expressing the bifurcation parameter b_1 as a function of the endemic state variable and performing a Taylor expansion about $x = 0$, we obtain a first-order approximation that characterizes the bifurcation direction. Solving (17) for b_1 yields

$$b_1 = b_1(x) := \frac{b_1^{(1)}}{b_1^{(2)}}, \tag{19}$$

where

$$\begin{aligned} b_1^{(1)} &= \big(\mu(1+\tilde{a}x)+\gamma\big)\Big(\alpha+\mu+b_2(1+vx)x\Big) \\ &\quad - (1+vx)b_2\gamma x - p\alpha\gamma, \\ b_1^{(2)} &= (1+vx)\Big[(1-x)(1+\tilde{a}x) \\ &\quad \times \Big(\alpha+\mu+b_2(1+vx)x\Big) - \gamma x\Big]. \end{aligned}$$

Clearly,

$$b_1(0) = b_1^*.$$

Differentiating (19) at $x = 0$, we obtain

$$\begin{aligned} b_1'(0) = \frac{1}{\alpha+\mu}\Big[&\tilde{a}\mu(\alpha+\mu) + b_2\mu \\ &- b_1^*\Big((\tilde{a}+v-1)(\alpha+\mu)+b_2-\gamma\Big)\Big]. \end{aligned} \tag{20}$$

Hence, in a neighborhood of $x = 0$,

$$b_1(x) = b_1^* + b_1'(0)x + \mathcal{O}(x^2).$$

This expansion determines the bifurcation direction:

- if $b_1'(0) > 0$, then $b_1 > b_1^*$ for sufficiently small $x > 0$. Consequently, the EE emerges when $\mathcal{R}_0 > 1$, and the bifurcation is forward;
- if $b_1'(0) < 0$, then $b_1 < b_1^*$ for sufficiently small $x > 0$. Consequently, a positive EE exists even when $\mathcal{R}_0 < 1$, and the bifurcation is backward.

The result is summarized in the following theorem.

Theorem 4. *Let b_1 be the bifurcation parameter, and let b_1^* be given by* (18)*. Then the EE branch near E_0 satisfies*

$$b_1 = b_1^* + b_1'(0)x_2^* + \mathcal{O}\big((x_2^*)^2\big),$$

where $b_1'(0)$ is given by (20)*. Consequently,*

(1) if $b_1'(0) > 0$, the bifurcation at $b_1 = b_1^*$ is forward;

(2) if $b_1'(0) < 0$, the bifurcation at $b_1 = b_1^*$ is backward.

The occurrence of backward bifurcation is promoted by mechanisms that enhance disease persistence following recovery, particularly relapse and reinfection. In particular, the parameters p, α, b_2, and the treatment saturation parameter $\tilde{a}$ appear explicitly in (20), indicating that they can alter the bifurcation direction even though some of them do not appear in the expression for the threshold parameter $\mathcal{R}_0$.

Because the model may exhibit backward bifurcation, establishing a complete global stability result for the DFE becomes considerably more challenging. In particular, the condition $\mathcal{R}_0 < 1$ is no longer sufficient to guarantee convergence to the DFE, since a stable EE may coexist with the DFE. Consequently, the global dynamics depend on the initial conditions, and a complete characterization of the global stability requires additional analysis beyond the scope of the present study.

5. Numerical simulations

This section presents numerical simulations that demonstrate and support the analytical results obtained in the previous sections. Specifically, we first estimate the model parameters using TB incidence data from Indonesia. We then analyze the dynamical behavior of the system through time-series simulations around the equilibria. Next, we investigate the sensitivity of the basic reproduction number using partial rank correlation coefficients and illustrate its dependence on key parameters through contour plots in selected parameter planes. Furthermore, we explore the epidemiological implications of the transmission rate b_1 by examining the epidemic size, peak timing, and peak prevalence. The nonlinear dynamics of the model are further characterized through forward and backward bifurcation diagrams with respect to b_1. Finally, we assess the numerical robustness of the proposed NSFD scheme under different time-step sizes and compare its performance with classical numerical methods, namely the forward Euler and fourth-order Runge–Kutta methods.

5.1. Parameter estimation

First, we estimate the parameter values of the NSFD model given by (5)–(6). To this end, we use annual TB incidence data (per 100,000 population) for Indonesia from 2000 to 2024, obtained from the World Bank database,[64] which is based on the World Health Organization (WHO) Global Tuberculosis Report. From the baseline model of

Aldila,[20] we adopt the parameter values $p = 0.5$, $v = 0.1$, and $\alpha = 0.2$. Meanwhile, according to United Nations data,[65] the average life expectancy in Indonesia over the period 2000–2024 is 68.62 years. Therefore, we set the natural mortality rate to $\mu = 1/68.62$. The time-step size of the NSFD scheme is fixed at $h = 1$. The remaining parameters, namely b_1, b_2, γ, $\tilde{a}$, and the initial conditions $x_{2,0}$ and $x_{3,0}$, are estimated.

Based on system (4), we define the dimensionless instantaneous incidence rate by

$$\mathcal{I}(x_2, x_3) = b_1(1 - x_2 - x_3)(1 + vx_2)x_2 + p\alpha x_3 + b_2(1 + vx_2)x_2x_3.$$

This expression coincides with F_n in (5), namely,

$$F_n = \mathcal{I}(x_{2,n}, x_{3,n}).$$

Here, F_n is referred to as the as model-predicted TB case incidence. Since the World Bank indicator reports new and relapse TB cases occurring each year, including the relapse term is appropriate. Reinfection is also incorporated by assuming that a reinfected recovered individual is counted as a new recurrent TB case in the model.

Let

$$\widehat{Y}_n = 10^5 F_n, \qquad n = 0, 1, 2, \ldots, 24,$$

be the model-predicted incidence per 100,000 people in year $2000 + n$, and let $\theta = (b_1, b_2, \gamma, \tilde{a}, x_{2,0}, x_{3,0})$ be the vector of parameters and initial conditions that needs to be estimated. The objective function for the parameter estimation procedure is

$$\mathcal{J}(\theta) = \sum_{n=0}^{24} \left[\frac{Y_n - \widehat{Y}_n(\theta)}{\max_j Y_j} \right]^2,$$

where Y_n is the TB incidence data for year $2000+n$.

We used the particle swarm optimization (PSO) algorithm[66] to estimate the vector θ that minimizes the objective function $\mathcal{J}(\theta)$. We utilized the PSO package function in MATLAB with the following specifications: swarm size 300, maximum iterations 500, maximum stall iterations 100, and function tolerance 10^{-10}. We set the parameter bounds for the estimation procedure as follows

$$10^{-5} \le b_1 \le 10, \quad 0 \le b_2 \le 10,$$
$$10^{-3} \le \gamma \le 5, \quad 0 \le \tilde{a} \le 1000,$$
$$10^{-6} \le x_{2,0} \le 0.05, \quad 0 \le x_{3,0} \le 0.5.$$

The PSO algorithm is terminated after reaching its maximum of 500 iterations. The convergence behaviour of the objective function $\mathcal{J}(\theta)$ is reported in **Figure 1**.

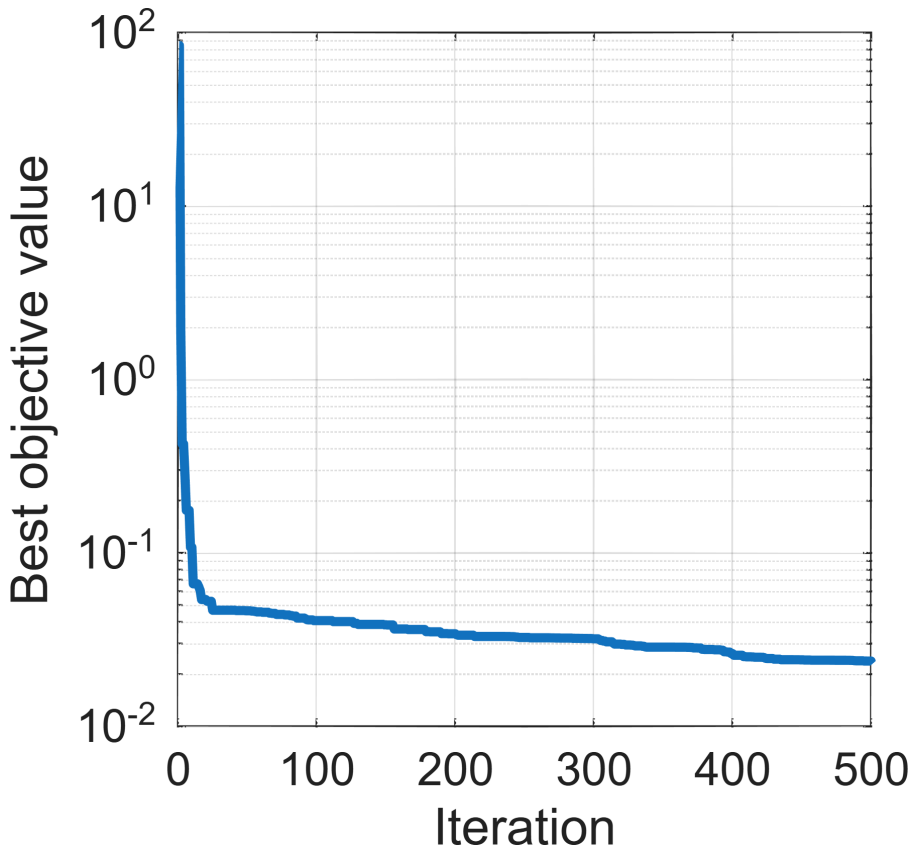


Figure 1. PSO convergence of the objective function $\mathcal{J}(\theta)$

After we obtained the estimated parameter values, we calculated three goodness-of-fit measures: root mean square error (RMSE), mean absolute percentage error (MAPE), and coefficient of determination (R^2):

$$\text{RMSE} = \sqrt{\frac{1}{25}\sum_{n=0}^{24}(Y_n - \widehat{Y}_n)^2},$$

$$\text{MAPE} = \frac{100\%}{25}\sum_{n=0}^{24}\left|\frac{Y_n - \widehat{Y}_n}{Y_n}\right|,$$

$$R^2 = 1 - \frac{\sum_{n=0}^{24}(Y_n - \widehat{Y}_n)^2}{\sum_{n=0}^{24}(Y_n - \bar{Y})^2},$$

where $\bar{Y}$ is the average of TB incidence data.

The results of the parameter estimation are provided in **Table 1**. The goodness-of-fit statistics indicate that the proposed NSFD model (6) provides a good representation of the observed TB incidence data. The model yields an RMSE of 11.95 indicating relatively small prediction errors. Moreover, the MAPE is only 2.56%, which corresponds to excellent predictive accuracy. The coefficient of determination, $R^2 = 0.7222$, shows that approximately 72.2% of the variability in the observed data is explained by the model. This result is supported by the plot of the model fit versus the observed data and the fitting residual in **Figure 2**. From the figure, it is observed that the TB incidence in Indonesia decreased steadily from 2000 to 2020, followed by a sharp increase between 2021 and 2023, before declining slightly in 2024. This change in trend may be associated with the impact of the COVID-19 pandemic, which began in 2020. Using parameter values from **Table 1**, the estimated basic reproduction number ($\mathcal{R}_0$) for the Indonesian TB data is $\mathcal{R}_0 \approx 0.2269$. It should be noted that the estimated parameters may be affected by the quality of the data for example underreporting, changes in diagnosis, and variation in TB case detection over time.

Table 1. Parameter and initial values of the NSFD model of TB (6) with bootstrap 95% confidence intervals and the goodness-of-fit of the parameter estimation

Parameter	**Value**	**Lower bound**	**Upper bound**	**Source**
b_1	0.0863	0.0803	0.1073	Estimated using PSO
b_2	6.0106	4.5974	9.9999	Estimated using PSO
γ	0.6846	0.0631	1.8544	Estimated using PSO
$\tilde{a}$	1000	2.22×10^{-14}	1000	Estimated using PSO
α	0.2			[20]
p	0.5			[20]
v	0.1			[20]
μ	1/68.62			UN data[65]
Initial condition				
$x_{2,0}$	1.00×10^{-6}	1.00×10^{-6}	0.0035	Estimated using PSO
$x_{3,0}$	0.0365	0.0248	0.0382	Estimated using PSO
Goodness-of-fit				
RMSE	11.9531			Calculated
MAPE	2.56%			Calculated
R^2	0.722			Calculated

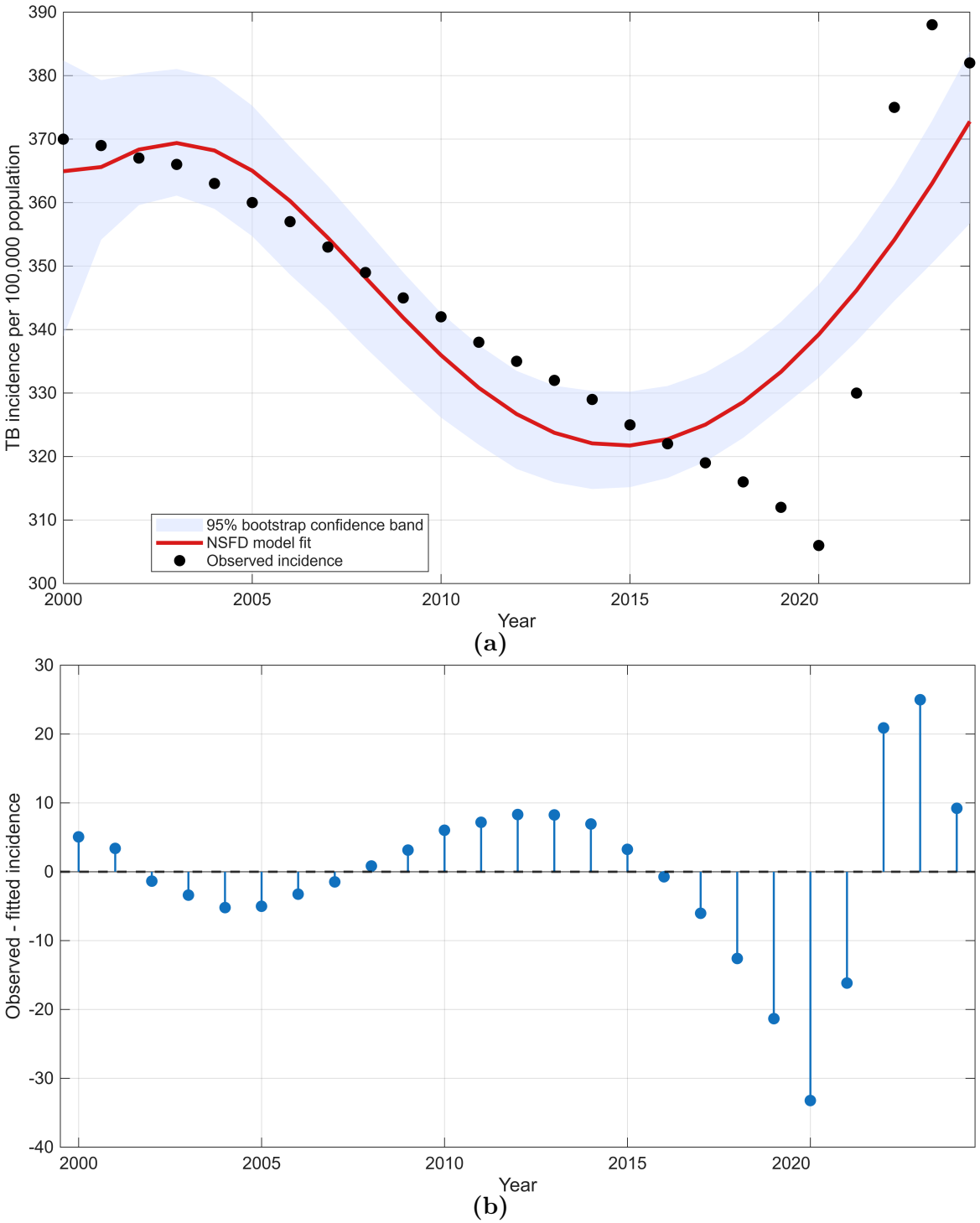


Figure 2. Data fitting of TB incidence in Indonesia from 2000–2024 using parameter values from **Table 1**. (a) The NSFD model fit versus the observed data with 95% bootstrap confidence interval. (b) The fitting residual.

5.2. Dynamics around equilibria

Figure 3 illustrates the time-series behavior of the proposed NSFD model (6) for three different values of the transmission rate b_1. In **Figure 3(a)**, where $\mathcal{R}_0 = 0.0263 < 1$, both the infected and recovered populations gradually converge to zero, confirming that the DFE is locally asymptotically stable. In contrast, **Figure 3(b)** shows that, although $\mathcal{R}_0 = 0.2269 < 1$, the infected population does not die out but instead converges to a positive steady state. This behavior confirms the occurrence of a backward bifurcation, in which a stable endemic equilibrium coexists with the DFE even when $\mathcal{R}_0 < 1$. Finally, **Figure 3(c)** shows that when $\mathcal{R}_0 = 1.3154 > 1$, the infected population rapidly converges to a positive endemic

equilibrium, while the recovered population approaches its corresponding steady-state value.

It should be noted that the high endemic level in **Figure 3(c)**, where x_2^* approaches one, does not represent the current epidemiological situation in Indonesia. The parameter value $b_1 = 0.5$ is selected to illustrate the qualitative behavior of the model when $\mathcal{R}_0 > 1$ and the solution converges to an EE. Current Indonesian TB data indicate a high disease burden, but not an infectious proportion close to the entire population. Moreover, the reported TB data correspond to annual incidence, whereas x_2 represents the proportion of the population in the infectious compartment; therefore, the two quantities are not directly comparable. Thus, **Figure 3(c)** is interpreted as an illustrative high-transmission scenario.

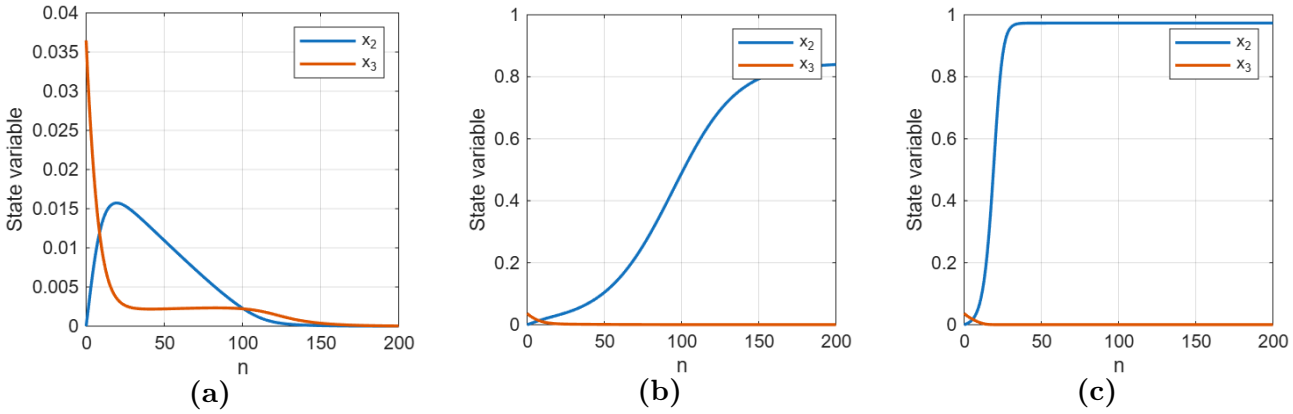


Figure 3. Time series of x_2 and x_3 when (a) the DFE is stable and $\mathcal{R}_0 = 0.0263 < 1$, (b) the DFE is unstable despite $\mathcal{R}_0 = 0.2269 < 1$, and (c) the EE is stable and $\mathcal{R}_0 = 1.3154 > 1$. We used the parameter values in **Table 1**, especially (a) $b_1 = 0.01$, (b) $b_1 = 0.0863$, and (c) $b_1 = 0.5$.

5.3. Sensitivity analysis of the basic reproduction number

Using the basic reproduction number ($\mathcal{R}_0$) as the threshold quantity, we perform a global sensitivity analysis to identify the model parameters that have the greatest influence on TB transmission. To this end, we employ the partial rank correlation coefficient (PRCC) method proposed by.[67] The PRCC values are computed using Latin hypercube sampling with 3000 samples. The model parameters are varied over biologically reasonable ranges centered around the baseline values given in **Table 1**:

$$0.001 \leq b_1 \leq 0.5,\ 0.1 \leq p \leq 0.9,\ 0.01 \leq \alpha \leq 0.5,$$
$$1/90 \leq \mu \leq 1/50,\ 0.1 \leq \gamma \leq 1.$$

Figure 4 presents the PRCC values of $\mathcal{R}_0$ with respect to the model parameters. It can be observed that b_1 and p exhibit strong positive correlations with $\mathcal{R}_0$, indicating that higher transmission and relapse rates substantially enhance disease transmission. In contrast, γ exhibits a strong negative correlation, suggesting that increasing the recovery rate effectively reduces the transmission potential. The parameter α has a moderate positive influence, whereas μ exhibits only a weak negative effect on $\mathcal{R}_0$. In general, the results identify b_1, γ, and p as the dominant parameters governing disease transmission, which is consistent with their prominent roles in the model. These findings suggest that TB control in Indonesia should prioritize reducing transmission and relapse while improving effective treatment. These three parameters are further examined through contour plots of the basic reproduction number.

To further investigate the interaction among the most influential parameters, we present contour plots of $\mathcal{R}_0$ in selected parameter planes. Specifically, we consider the parameter pairs (b_1, γ), (b_1, p), and (γ, p). **Figure 5** illustrates the dependence of $\mathcal{R}_0$ on these parameter pairs. **Figure 5(a)** shows that $\mathcal{R}_0$ increases with b_1 and decreases with γ, reflecting that higher transmission rates promote disease spread, whereas higher recovery rates suppress transmission. **Figure 5(b)** shows that $\mathcal{R}_0$ increases as both b_1 and p increase, indicating that transmission and relapse reinforce each other in sustaining disease spread. Conversely, **Figure 5(c)** shows that $\mathcal{R}_0$ decreases as γ increases and increases as p increases, illustrating the opposite effects of recovery and relapse on disease transmission. These contour plots provide a clear visualization of the threshold condition $\mathcal{R}_0 = 1$.

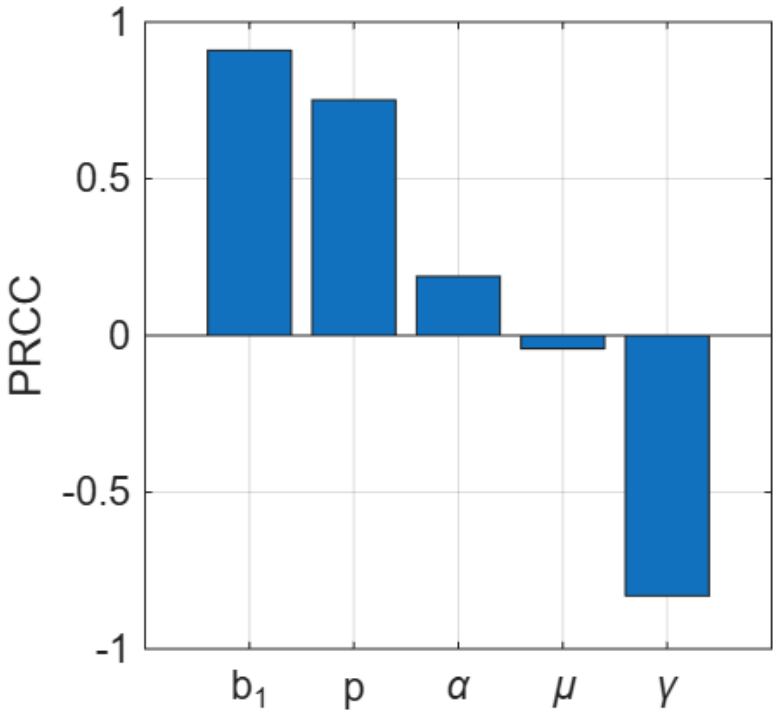


Figure 4. Partial rank correlation coefficients (PRCC) of the basic reproduction number $\mathcal{R}_0$ with respect to the model parameters

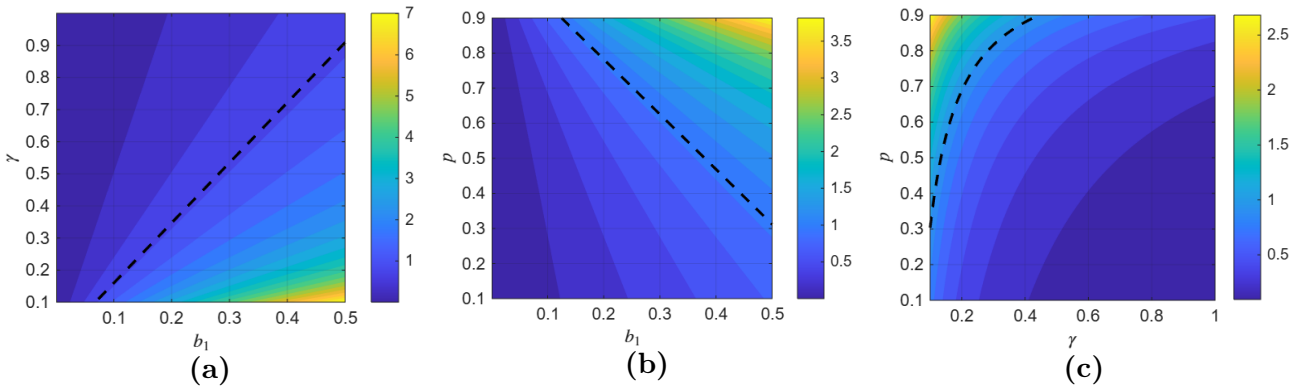


Figure 5. Contour plots of the basic reproduction number $\mathcal{R}_0$ in (a) the (b_1, γ) plane, (b) the (b_1, p) plane, and (c) the (γ, p) plane. The dashed curves represent the threshold $\mathcal{R}_0 = 1$. The other parameter values are given in **Table 1**.

5.4. Epidemiological outcomes

The results of the previous subsection identify b_1 as the most influential parameter. We now investigate its impact on three epidemiological outcomes: epidemic size, peak timing, and peak prevalence.

To this end, for each value of b_1, we compute three epidemiological quantities from the numerical solution. The epidemic size is defined as the cumulative infectious burden,

$$\mathcal{E} = \sum_{n=0}^{M} x_{2,n},$$

the peak prevalence is

$$P = \max_{0 \le n \le M} x_{2,n},$$

and the peak timing is

$$T_p = \arg\max_{0 \le n \le M} x_{2,n}.$$

Figure 6 illustrates the dependence of these epidemiological outcomes on the transmission rate b_1. Throughout this analysis, we set $M = 400$. As shown in **Figure 6(a)**, the epidemic size increases monotonically with b_1, indicating that higher transmission rates result in a substantially greater cumulative infectious burden. This suggests that even relatively small increases in the

transmission rate can, over time, lead to a considerably larger epidemic.

Figure 6(b) shows a nonlinear relationship between b_1 and the peak timing. For small values of b_1, the disease is rapidly eliminated without producing a major outbreak. As b_1 increases to intermediate values, the epidemic peak occurs later, indicating more sustained disease transmission and a longer epidemic duration. For larger values of b_1, the peak occurs much earlier, corresponding to a rapid and more explosive outbreak. This transition reflects a threshold-type behavior around the critical value b_1^*, consistent with the bifurcation analysis.

Figure 6(c) shows that the peak prevalence increases with b_1, indicating that a larger proportion of the population becomes infected at the epidemic peak. From a public health perspective, this finding is particularly important because higher peak prevalence places greater pressure on healthcare resources and service capacity. Overall, these results demonstrate that b_1 plays a central role not only in determining whether an outbreak occurs, but also in shaping its magnitude, duration, and timing. Therefore, interventions aimed at reducing b_1, such as strengthening infection control measures, reducing effective contact, improving treatment effectiveness, and enhancing early case detection, are essential for reducing the overall epidemic burden, delaying or preventing the epidemic peak, and alleviating pressure on healthcare systems.

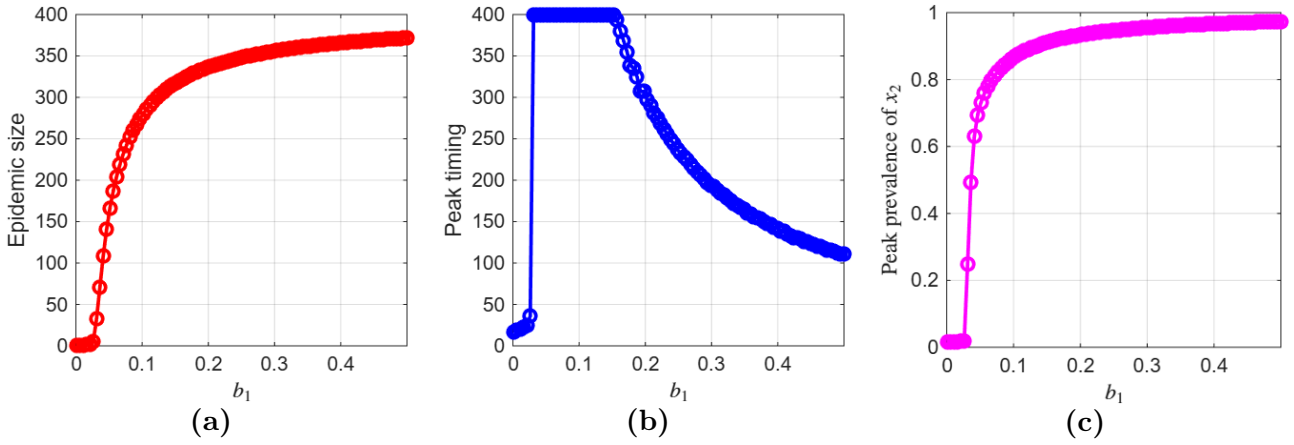


Figure 6. Epidemiological outcomes, such as (a) epidemic size, (b) peak timing, and (c) peak prevalence, as functions of the transmission rate b_1. The other parameter values are given in **Table 1**.

5.5. Bifurcation diagrams

Here, we verify the bifurcation analysis presented in Theorem 4 by illustrating both forward and backward bifurcations using parameter sets that produce positive and negative values of $b_1'(0)$, respectively. To illustrate a forward bifurcation, we select a parameter set satisfying $b_1'(0) > 0$. Conversely, to illustrate a backward bifurcation, we choose a parameter set satisfying $b_1'(0) < 0$. All simulations are performed using the time-step size $h = 1$. **Figure 7** illustrates the bifurcation behavior of the endemic equilibrium x_2^* as the transmission parameter b_1 varies.

Figure 7(a) shows a forward bifurcation, where the EE emerges continuously from the DFE at the critical threshold $b_1 = b_1^*$. For $b_1 < b_1^*$, only the DFE exists and is locally asymptotically stable. When $b_1 > b_1^*$, a unique stable EE appears and increases smoothly as b_1 increases. In contrast, **Figure 7(b)** exhibits a backward bifurcation, characterized by the coexistence of multiple equilibria for $b_1 < b_1^*$. This indicates that a stable EE may persist even below the threshold, implying that reducing b_1 below b_1^* alone is insufficient to eliminate the disease. This phenomenon reflects bistability and suggests that more stringent control measures are required to drive the system toward the DFE. The occurrence of backward bifurcation has also been reported in the baseline model of Aldila,[20] where the treatment rate is assumed to be linear.

From an epidemiological perspective, backward bifurcation implies that reducing the basic reproduction number below unity may not be sufficient to eliminate TB, since a stable endemic equilibrium can persist when $\mathcal{R}_0 < 1$. Therefore, TB control should combine transmission-reduction measures with interventions that reduce relapse, reinfection, and the number of existing infectious individuals through early detection and effective treatment.

We emphasize that the parameter sets used in **Figure 7** are selected to illustrate the forward

and backward bifurcation structures. In particular, the use of $\tilde{a} = 1$ does not satisfy the sufficient condition (8) of Theorem 1. In **Figure 7(a)**, we instead consider the equilibrium branches obtained from the algebraic equilibrium equations and retain only biologically admissible equilibria satisfying $x_2^* \geq 0$, $x_3^* \geq 0$, and $x_2^* + x_3^* \leq 1$. Hence, **Figure 7** is intended to illustrate the equilibrium and bifurcation structure. In **Figure 7(b)**, under the parameter values in **Table 1**, we also report that the bistable region for the basic reproduction number is $0.045 \lesssim \mathcal{R}_0 < 1$. A larger treatment saturation parameter $\widetilde{a}$ weakens the effective treatment response at high infection levels and may promote backward bifurcation and bistability.

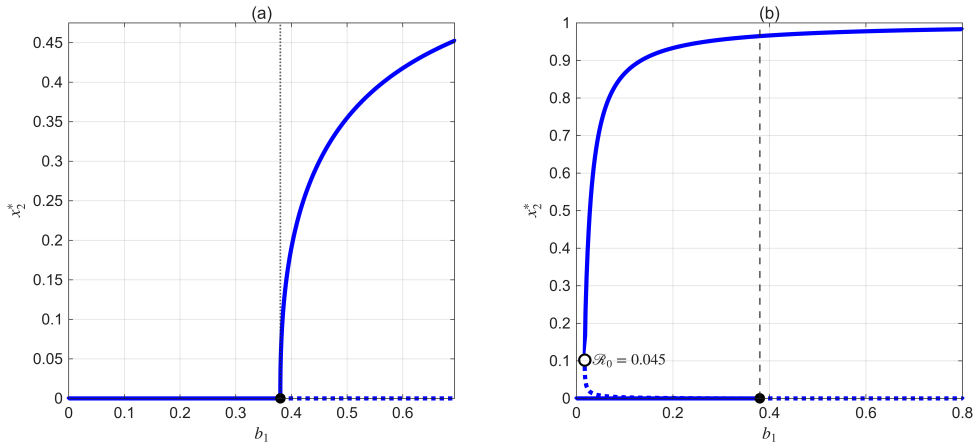


Figure 7. Bifurcation diagrams of the endemic equilibrium (x_2^*) with respect to the transmission rate b_1 for (a) forward bifurcation and (b) backward bifurcation. The black dashed line indicates the threshold $b_1^* = 0.3801$. The blue solid line is for stable equilibria, and the blue dashed line is for unstable equilibria. The remaining parameter values are given in **Table 1**, except $b_2 = 0.7$ and $\tilde{a} = 1$ in panel (a).

5.6. NSFD robustness and comparison with other schemes

Since this study employs an NSFD scheme, it is important to examine its numerical robustness for different time-step sizes. **Figure 8** demonstrates the robustness of the proposed NSFD scheme for time-step sizes ranging from $h = 0.1$ to $h = 5.0$. In both panels, the solutions converge to the same equilibrium values regardless of the different time-step sizes. This indicates that the proposed discretization preserves the qualitative behavior of the underlying co ntinuous model for any choice of h. Although smaller values of h lead to slower convergence, all trajectories remain positive and bounded while converging to the same EE. These results demonstrate that the proposed NSFD scheme is dynamically consistent and numerically stable even for relatively large time-step sizes.

Further observations are depicted in **Figure 9**, which compares the numerical solutions obtained using the proposed NSFD scheme (6), the forward Euler method, and the fourth-order Runge–Kutta (RK4) method for two different time-step sizes. For the relatively small step size $h = 0.1$, all three schemes produce stable and almost identical time-series solutions for both x_2 and x_3, indicating that they accurately approximate the continuous model. However, when the step size is increased to $h = 5$, the numerical behavior becomes significantly different. The proposed NSFD scheme still produces stable, positive, and bounded solutions, whereas the forward Euler and RK4 methods fail to preserve these qualitative properties. In particular, the RK4 method generates negative values for the infected population and exhibits unrealistic growth in the recovered population, while the forward Euler method also deviates from the NSFD solution. These results demonstrate that the proposed NSFD scheme is more robust than the forward Euler and RK4 methods for large time-step sizes. Our findings are consistent with previous studies, which also reported that the NSFD scheme is superior to conventional numerical methods in preserving the qualitative properties of the underlying continuous model.[68–70]

To verify that the assumptions of Theorem 1 are satisfied for the numerical experiment in **Figure 9**, we use the parameter values in **Table 1** together with $r = 0.05$. The estimated initial condition also satisfies $x_{3,0} = 0.0365 < 0.05(1 - 10^{-6})$, so that $(x_{2,0}, x_{3,0}) \in \Omega_{0.05}$. First, $b_2 = 6.0106 > b_1 = 0.0863$. Moreover, $d_r = 0.382515$, and hence $rp\alpha + (1+v)d_r = 0.4257665 < 1$. Furthermore, $\psi_0 = 0.2085001$, whereas $\psi_1 = 3.1489364$. Since $\mu = \frac{1}{68.62} = 0.0145730$, we

have $\min\{\mu, \psi_0, \psi_1\} = 0.0145730$. Therefore, $r\min\{\mu, E_0, E_1\} = 7.2865 \times 10^{-4}$, while $\frac{(1-r)\gamma}{\widetilde{a}} = 6.5037 \times 10^{-4}$. Thus, $r\min\{\mu, E_0, E_1\} > \frac{(1-r)\gamma}{\widetilde{a}}$. Hence, all conditions of Theorem 1 are satisfied for the parameter values used in **Figure 8**. Since the theorem holds for every $h > 0$, it applies in particular to both step sizes considered in **Figure 8**, namely $h = 0.1$ and $h = 5$. Therefore, the NSFD trajectories starting from the estimated initial condition remain in $\Omega_{0.05} \subset \Omega$, and consequently preserve nonnegativity and the biological feasibility condition $x_{2,n} + x_{3,n} \leq 1$ for all $n \geq 0$.

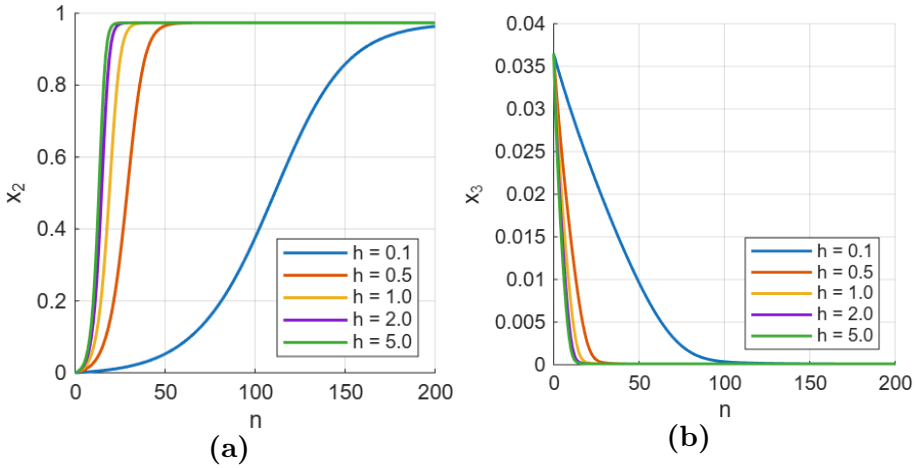


Figure 8. Robustness of the NSFD scheme with respect to the step size h for variables (a) x_2 and (b) x_3. The other parameter values are given in **Table 1**.

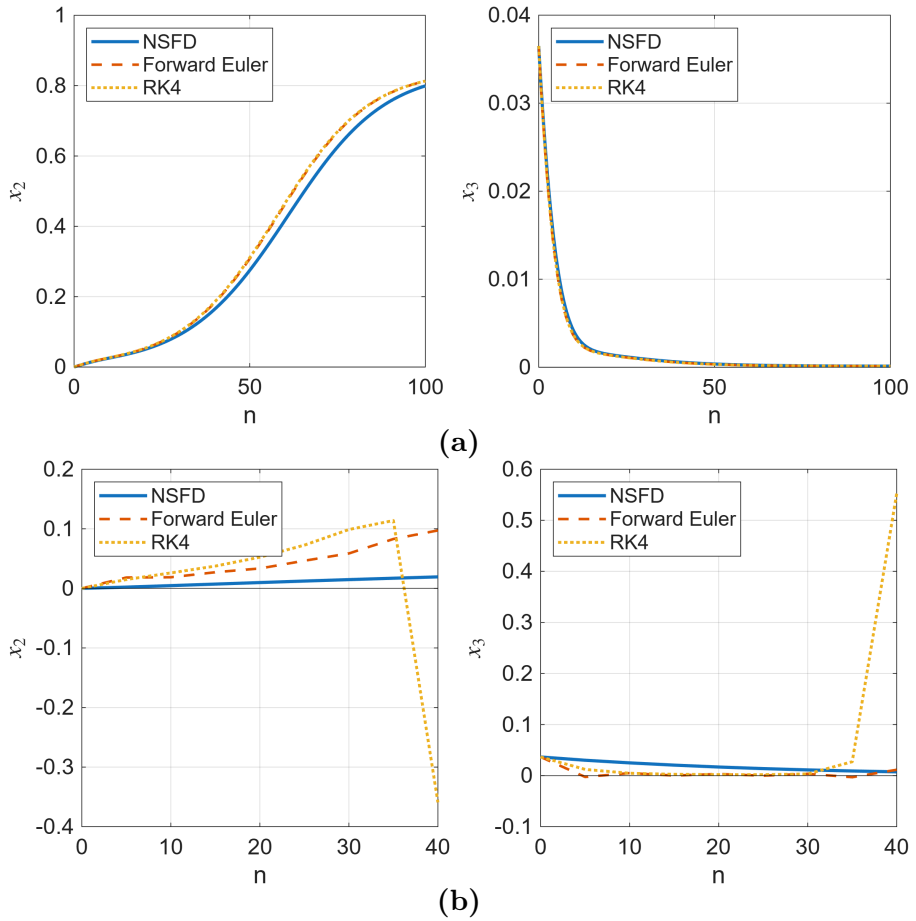


Figure 9. Time-series comparison of x_2 and x_3 obtained using the proposed NSFD scheme, the forward Euler method, and the fourth-order Runge–Kutta (RK4) method for two different time-step sizes: (a) $h = 0.1$ and (b) $h = 5$. The other parameter values are given in **Table 1**.

6. Conclusion

In this study, a discrete-time tuberculosis (TB) model was developed using a nonstandard finite difference (NSFD) scheme based on a continuous model incorporating relapse, reinfection, nonlinear incidence, and saturated treatment. The proposed NSFD scheme preserves the essential qualitative properties of the continuous model, including boundedness, positivity, and the invariance of the feasible region, while remaining consistent with the biological interpretation of the disease dynamics.

The analysis showed that the NSFD model shares the same basic reproduction number as the corresponding continuous model and exhibits identical local stability properties of the disease-free equilibrium. Moreover, the model can exhibit both forward and backward bifurcations, which have also been reported in the baseline model of Aldila,[20] where the treatment rate is assumed to be linear. In particular, the combined effects of relapse, reinfection, and saturated treatment may give rise to backward bifurcation, leading to bistability and disease persistence even when the basic reproduction number is less than one. This finding indicates that reducing the basic reproduction number below unity alone may not be sufficient to eliminate TB and that more comprehensive intervention strategies may be required.

Using TB incidence data from Indonesia for the period 2000–2024, we estimated the model parameters. The analytical results were further supported by numerical simulations, which demonstrated the dynamical behavior around the equilibria, the global sensitivity of the basic reproduction number, and the dependence of key epidemiological outcomes on the transmission parameter. The proposed NSFD scheme was shown to be robust with respect to the time-step size and to outperform classical numerical methods such as the forward Euler and fourth-order Runge–Kutta methods.

The main limitations are the absence of HIV co-infection, age structure, drug-resistant TB, and population heterogeneity. The model also assumes homogeneous mixing and uses a reduced three-compartment structure, so it does not explicitly represent latent infection, diagnosis stages, or detailed treatment pathways. Future work may extend the proposed model by addressing those limitations or by adding optimal control strategies into the discrete model to further enhance its realism and applicability.

Acknowledgments

None.

Funding

This research is funded by the Indonesian Endowment Fund for Education (LPDP) on behalf of the Indonesian Ministry of Higher Education, Science and Technology and managed under the EQUITY Program (Contract No. 4306/B3/DT.03.08/2025).

Conflict of interest

The author declares there are no competing interests.

Author contributions

This is a single-authored article.

Availability of data

All data supporting the findings of this study are available within the paper along with original reference. The MATLAB code is available upon reasonable request from the corresponding author. The Indonesian TB incidence data are publicly and freely available from the World Bank database.[64]

AI tools statement

This manuscript used ChatGPT (OpenAI) for minor language corrections to improve grammar and readability. All intellectual content, conceptual development, and analyses were solely the work of the author.

References

1. Xu C, Luo H. *Risks of Tuberculosis Prevention and Control*. Singapore: Springer; 2021. https://doi.org/10.1007/978-981-33-6958-0_5
2. Yu WY, Wang YX, Mei JZ, Hu FX, Ji LC. *Overview of Tuberculosis*. Singapore: Springer; 2019. https://doi.org/10.1007/978-981-32-9763-0_1
3. Sadigurschi G, Cuschni MC, Dos Santos EAP, *et al.* Challenges in developing new tuberculosis vaccines. *Mem Inst Oswaldo Cruz.* 2025;120:02760240236. https://doi.org/10.1590/0074-02760240236
4. Hernández-Acevedo GN, González-Vázquez R, Reyes-Pavón D, Torres-Maravilla E. Tuberculosis infection and comorbidities: A public health issue in Baja California, Mexico. *Bacteria.* 2024;3(3):194-208. https://doi.org/10.3390/bacteria3030014

5. Gwebu AB, Naidoo C, Wright CY. Socio-demographic and environmental factors associated with tuberculosis infection among children less than 15 years in Hhohho region of Eswatini (Swaziland). *Front Environ Health.* 2026;5:1738173. https://doi.org/10.3389/fenvh.2026.1738173
6. Xue Y, Zhou J, Wang P, *et al.* Burden of tuberculosis and its association with socio-economic development status in 204 countries and territories, 1990-2019. *Front Med (Lausanne).* 2022;9:905245. https://doi.org/10.3389/fmed.2022.905245
7. Sotgiu G, Sulis G, Matteelli A. Tuberculosis: A World Health Organization perspective. *Microbiol Spectr.* 2017;5(1). https://doi.org/10.1128/microbiolspec.TNMI7-0036-2016
8. Katzman JH, Sampson M, Casañas B. *Tuberculosis: Advances in Diagnostics and Treatment.* Cham, Switzerland: Springer International Publishing; 2019. https://doi.org/10.1007/978-3-030-29022-1_19
9. Sotgiu G, Glaziou P, Sismanidis C, Raviglione M. *Tuberculosis Epidemiology.* Amsterdam, Netherlands: Elsevier; 2016. https://doi.org/10.1016/B978-0-12-803678-5.00507-5
10. Jain A, Dixit P. *Challenges in Management of Tuberculosis in Developing Countries.* Sharjah, UAE: Bentham Science Publishers; 2012. https://doi.org/10.2174/978160805292911201010090
11. Lv X, Ji X, Xiong L, Chen Y, Wang H, Yang Y. Global prevalence of tuberculosis and drug-resistant forms: A 30-year analysis from 1990 to 2019. *J Glob Antimicrob Resist.* 2025;44:411-419. https://doi.org/10.1016/j.jgar.2025.07.012
12. Barker RD. Clinical tuberculosis. *Medicine (Baltimore).* 2016;44(6):384-389. https://doi.org/10.1016/j.mpmed.2016.03.002
13. Rojano B, Caminero J, Hayek M. Curving tuberculosis: Current trends and future needs. *Ann Glob Health.* 2019;85(1):106. https://doi.org/10.5334/aogh.2415
14. Guimarães RM, Lobo APD, Siqueira EAF, Borges TFF, Melo SCC. Tuberculosis, HIV, and poverty: Temporal trends in Brazil, the Americas, and worldwide. *J Bras Pneumol.* 2012;38(4):511-517. https://doi.org/10.1590/S1806-37132012000400014
15. Okuonghae D, Korobeinikov A. *Dynamics of Tuberculosis in a Developing Country: Nigeria as a Case Study.* New York, NY: Springer; 2013. https://doi.org/10.1007/978-1-4614-9224-5_3
16. Kirschner D, Pienaar E, Marino S, Linderman JJ. A review of computational and mathematical modeling contributions to our understanding of mycobacterium tuberculosis within-host infection and treatment. *Curr Opin Syst Biol.* 2017;3:170-185. https://doi.org/10.1016/j.coisb.2017.05.014
17. Abiodun OE, Olayiwola MO. Analysis of tuberculosis infection dynamics using Caputo fractional-order models with diagnosis and treatment interventions. *Tuberculosis (Edinb).* 2025;155:102694. https://doi.org/10.1016/j.tube.2025.102694
18. Manivel M. Impact of vaccination and reinfection on tuberculosis dynamics under fractional-order modeling. *Discov Public Health.* 2026;23(1):52. https://doi.org/10.1186/s12982-026-01352-z
19. Kuddus MA, Meehan MT, Sayem MA, McBryde ES. Scenario analysis for programmatic tuberculosis control in Bangladesh: A mathematical modelling study. *Sci Rep.* 2021;11(1):83768. https://doi.org/10.1038/s41598-021-83768-y
20. Aldila D. Change in stability direction induced by temporal interventions: A case study of a tuberculosis transmission model with relapse and reinfection. *Front Appl Math Stat.* 2025;11:1541981. https://doi.org/10.3389/fams.2025.1541981
21. Wijayanti SN, Widowati, Kartono, Sutrisno. Integrating disease dynamics and environmental sanitation: A mathematical model of tuberculosis spread in communities with compromised water and waste management. *Proc Sci.* 2025;196:3002. https://doi.org/10.1051/bioconf/202519603002
22. Gemeda AE, Obsu LL, Gurmu ED, Degefa TS. Mathematical modeling of tuberculosis transmission dynamics with vaccination and two lines of treatments: A Caputo fractional approach. *J Appl Math Comput.* 2025;71(2):2017-2049. https://doi.org/10.1007/s12190-024-02308-9
23. Adi Y, Septian S. Dynamics of a fractional-order model for mycobacterium tuberculosis with Caputo-Fabrizio derivatives. *Nonlinear Dyn Syst Theory.* 2025;25(4):361-372. Accessed July 15, 2026. http://www.e-ndst.kiev.ua/v25n4/2(100)a.pdf
24. Chadhar K, Kishore J, Jani A, Shekhar C, Jani KK, Gupta N. Is isolation of open active pulmonary tuberculosis cases the last mile strategy to achieve tuberculosis elimination in India? *J Commun Dis.* 2025;57(3):182-190. https://doi.org/10.24321/0019.5138.202585
25. Menzies NA, Parriott A, Shrestha S, *et al.* Comparative modeling of tuberculosis epidemiology and policy outcomes in California. *Am J Respir Crit Care Med.* 2020;201(3):356-365. https://doi.org/10.1164/rccm.201907-1289OC
26. Saputra HL, Ansori MF. Analysis of an SVEIR with reinfection model of tuberculosis disease spread with saturated infected rate and imperfect vaccination. *AppliedMath.* 2025;5(4):163. https://doi.org/10.3390/appliedmath5040163
27. Elhia M, Balatif O, Boujallal L, Rachik M. Optimal control problem for a tuberculosis model with multiple infectious compartments and time delays. *Int J Optim Control Theor Appl.*

2021;11(1):75-91.
https://doi.org/10.11121/ijocta.01.2021.00885

28. Aldila D, Saslia BR, Gayatri W, H. Backward bifurcation analysis on tuberculosis disease transmission with saturated treatment. *J Phys Conf Ser*. 2021;1821:012002.
https://doi.org/10.1088/1742-6596/1821/1/012002
29. Aldila D, Chukwue V, Ginting ED, *et al*. Backward bifurcation and periodic dynamics in a tuberculosis model with integrated control strategies. *Math Biosci Eng*. 2025;22(10):2720-2760.
https://doi.org/10.3934/mbe.2025100
30. Ansori MF. Dynamical analysis and optimal control of a tuberculosis-diabetes comorbidity model with reinfection and relapse. *Chaos Theory Appl*. 2026;8(2):146-161.
https://doi.org/10.51537/chaos.1936957
31. Srivastava A, Srivastava PK. A tuberculosis model incorporating the impact of information, saturated treatment and multiple reinfections. *Eur Phys J Plus*. 2023;138(12):1075.
https://doi.org/10.1140/epjp/s13360-023-04754-z
32. Helikumi M, Daudi S, Lusekelo E, Mushayabasa S. Modeling and analyzing the impact of limited medical resources and mutation on tuberculosis dynamics. *Franklin Open*. 2024;9:100186.
https://doi.org/10.1016/j.fraope.2024.100186
33. Peter OJ, Aldila D, Ayoola TA, Balogun GB, Oguntolu FA. Modeling tuberculosis dynamics with vaccination and treatment strategies. *Sci Afr*. 2025;28:e02647.
https://doi.org/10.1016/j.sciaf.2025.e02647
34. Biswas M, Nairagi RK. Discretization of an eco-epidemiological model and its dynamic consistency. *J Differ Equ Appl*. 2017;23(5):860-877.
https://doi.org/10.1080/10236198.2017.1304544
35. Dang QA, Hoang MT, Trejos DY, Valverde JC. Nonstandard finite difference schemes for the study of the dynamics of the babesiosis disease. *Symmetry*. 2020;12(9):1447.
https://doi.org/10.3390/sym12091447
36. Mickens RE. Nonstandard finite difference schemes for differential equations. *J Differ Equ Appl*. 2002;8(9):823-847.
https://doi.org/10.1080/1023619021000000807
37. Mickens RE. *Advances in the Applications of Nonstandard Finite Difference Schemes*. Singapore: World Scientific; 2005.
https://doi.org/10.1142/5884
38. Mickens RE. Dynamic consistency: A fundamental principle for constructing nonstandard finite difference schemes for differential equations. *J Differ Equ Appl*. 2005;11(7):645-653.
https://doi.org/10.1080/10236190412331334527
39. Mickens RE. Calculation of denominator functions for nonstandard finite difference schemes for differential equations satisfying a positivity condition. *Numer Methods Partial Differ Equ*. 2007;23(3):672-691.
https://doi.org/10.1002/num.20198
40. Cui Q, Yang X, Zhang Q. An NSFD scheme for a class of SIR epidemic models with vaccination and treatment. *J Differ Equ Appl*. 2014;20(3):416-422.
https://doi.org/10.1080/10236198.2013.844802
41. Kathiri SA, Abdullah FA, Hamid NNA, Bashier E, Bhat AA, Sunny D. Applications of the non-standard finite difference method to a fractional modeling diabetes mellitus and its complications. *Contemp Math*. 2024;5(4):6296-6319.
https://doi.org/10.37256/cm.5420245701
42. Rafiq M, Arif M, Raza A, Khatoon Z. Numerical modeling of toxoplasmosis disease transmission dynamics. In: *Proceedings of the 15th International Bhurban Conference on Applied Sciences and Technology (IBCAST)*. Piscataway, NJ: IEEE; 2018:188-193.
https://doi.org/10.1109/IBCAST.2018.8312221
43. Conte D, Guarino N, Pagano G, Paternoster B. Positivity-preserving and elementary stable non-standard method for a COVID-19 SIR model. *Dolomites Res Notes Approx*. 2022;15(5):65-77.
https://doi.org/10.14658/pupj-drna-2022-5-7
44. Roeger LIW. Dynamically consistent discrete-time SI and SIS epidemic models. *Discrete Contin Dyn Syst Ser S*. 2013;2013:653-662.
https://doi.org/10.3934/proc.2013.2013.653
45. Darti I, Suryanto A, Hartono M. Global stability of a discrete SIR epidemic model with saturated incidence rate and death induced by the disease. *Commun Math Biol Neurosci*. 2020;2020:47.
https://doi.org/10.28919/cmbn/4710
46. Arif MS, Abodayeh K, Nawaz Y. Precision in disease dynamics: Finite difference solutions for stochastic epidemics with treatment cure and partial immunity. *Partial Differ Equ Appl Math*. 2024;9:100660.
https://doi.org/10.1016/j.padiff.2024.100660
47. Arif MS, Abodayeh K, Nawaz Y. A reliable computational scheme for stochastic reaction-diffusion nonlinear chemical model. *Axioms*. 2023;12(5):460.
https://doi.org/10.3390/axioms12050460
48. Yıldız TA. A comparison of some control strategies for a non-integer order tuberculosis model. *Int J Optim Control Theor Appl*. 2019;9(3):21-30.
https://doi.org/10.11121/ijocta.01.2019.00657
49. Nandi TR, Saha AK, Roy S. Analysis of a fractional order epidemiological model for tuberculosis transmission with vaccination and reinfection. *Sci Rep*. 2024;14:28290.
https://doi.org/10.1038/s41598-024-73392-x
50. Khan A, Shah K, Abdeljawad T, Amacha I. Fractal fractional model for tuberculosis: Existence and numerical solutions. *Sci Rep*. 2024;14:12211.
https://doi.org/10.1038/s41598-024-62386-4

51. Bhatter S, Kumawat S, Purohit SD, Suthar DL. Mathematical modeling of tuberculosis using Caputo fractional derivative: A comparative analysis with real data. *Sci Rep.* 2025;15:12672. https://doi.org/10.1038/s41598-025-97502-5
52. Bhatia B, Bhatter S, Purohit SD, Baleanu D, Suthar DL. A fractional model based on Caputo derivative for tuberculosis transmission using real data from Kenya. *Sci Rep.* 2026;16:1725. https://doi.org/10.1038/s41598-025-31440-0
53. Sutimin, Herdiana R, Utomo RHS, Permatasari AH. Stability analysis of tuberculosis epidemic model with saturated infection force. *EDP Sci.* 2020;202:12023. https://doi.org/10.1051/e3sconf/202020212023
54. Sulayman F, Abdullah FA. Analysis of a tuberculosis infection model considering the influence of saturated recovery (treatment). *Complexity.* 2021;2021:1805651. https://doi.org/10.1155/2021/1805651
55. Cao H, Song B, Zhou Y. Treatment strategies for the latent tuberculosis infections. *J Math Biol.* 2023;86(6):73. https://doi.org/10.1007/s00285-023-01927-3
56. Das S, Srivastava PK, Biswas P. Exploring Hopf bifurcations and endemic bubbles in a tuberculosis model with behavioral changes and treatment saturation. *Chaos.* 2024;34(1):017935. https://doi.org/10.1063/5.0179351
57. Rasheed S, Iyiola OS, Oke SI, Wade BA. Numerical and theoretical treatments of the optimal control model for the interaction between diabetes and tuberculosis. *Algorithm.* 2025;18(6):225. https://doi.org/10.3390/a18060348
58. Khoda P, Sarkar T, Prasad NS, Meena OP. Impact of media awareness, treatment saturation, and LTBI control on tuberculosis transmission: A mathematical modeling approach. *Comput Appl Math.* 2026;45(3):87. https://doi.org/10.1007/s40314-025-03543-x
59. Jury EI. A note on the modified stability table for linear discrete-time systems. *IEEE Trans Circuits Syst.* 1991;38(2):221-223. https://doi.org/10.1109/31.68301
60. Diekmann O, Heesterbeek JAP, Metz JAJ. On the definition and the computation of the basic reproduction ratio R_0 in models for infectious diseases in heterogeneous populations. *J Math Biol.* 1990;28(4):365-382. https://doi.org/10.1007/BF00178324
61. van den Driessche P, Watmough J. Reproduction numbers and sub-threshold endemic equilibria for compartmental models of disease transmission. *Math Biosci.* 2002;180(1-2):29-48. https://doi.org/10.1016/S0025-5564(02)00108-6
62. Kuznetsov YA. *Elements of Applied Bifurcation Theory.* 4th ed. Cham, Switzerland: Springer; 2023. https://doi.org/10.1007/978-3-031-22007-4
63. Elaydi SN. *An Introduction to Difference Equations.* 3rd ed. New York, NY: Springer; 2005. https://doi.org/10.1007/0-387-27602-5
64. Incidence of tuberculosis (per 100,000 people)–Indonesia. World Bank Open Data. Accessed July 15, 2026. https://data.worldbank.org/indicator/SH.TBS.INCD?locations=ID
65. World Population Prospects 2024: The 2024 Revision. United Nations, Department of Economic and Social Affairs, Population Division. Accessed July 15, 2026. https://population.un.org/wpp/
66. Kennedy J, Eberhart R. Particle swarm optimization. In: *Proceedings of ICNN'95 - International Conference on Neural Networks.* Vol 4. Piscataway, NJ: IEEE; 1995:1942-1948. https://doi.org/10.1109/ICNN.1995.488968
67. Marino S, Hogue IB, Ray CJ, Kirschner DE. A methodology for performing global uncertainty and sensitivity analysis in systems biology. *J Theor Biol.* 2008;254(1):178-196. https://doi.org/10.1016/j.jtbi.2008.04.011
68. Zeb S, Yatim SAM, Kamran A, Zulfiqar S, Rafiq M, Mohamad Noor N. A nonlinear delay mathematical model for predicting chlamydia dynamics and intervention effects. *Commun Biomath Sci.* 2025;8(2):132-164. https://doi.org/10.5614/cbms.2025.8.2.1
69. Zeb S, Yatim SAM, Kamran A, Kausar R, Rafiq M. A new delayed SEIR-SEI model for dengue transmission control with sensitivity and competitive mathematical analysis. *Comput Methods Differ Equ.* 2026;14(1):470-501. https://doi.org/10.22034/cmde.2025.67008.3176
70. Zeb S, Yatim SAM, Rafiq M, Raza A, Lampart M, Kamran A. Stepwise development and mathematical analysis of delayed dengue transmission models with control strategies. *Discov Public Health.* 2026;23:283. https://doi.org/10.1186/s12982-026-01583-0

Moch. Fandi Ansori *earned a Doctoral degree in Mathematics from Institut Teknologi Bandung, Indonesia in 2021. He is currently an Assistant Professor in the Department of Mathematics at Universitas Diponegoro, Indonesia. His research interest includes mathematical modeling of infectious disease dynamics using continuous and discrete-time models.*
https://orcid.org/0000-0002-4588-3885

An International Journal of Optimization and Control: Theories & Applications (https://accscience.com/journal/ijocta)



This work is licensed under a Creative Commons Attribution 4.0 International License. The authors retain ownership of the copyright for their article, but they allow anyone to download, reuse, reprint, modify, distribute, and/or copy articles in IJOCTA, so long as the original authors and source are credited. To see the complete license contents, please visit http://creativecommons.org/licenses/by/4.0/.